Application of a Twin-plane Electrical Capacitance Tomography Sensor for Characterising Bubble Behaviour in a Gas-solids Fluidized Bed

Xiaoxu LI, Artur J. JAWORSKI, and Xiaoan MAO

***Abstract*—Fluidized beds have been used extensively in general chemical engineering applications. However, due to their complex hydrodynamic characteristics, conventional measurement techniques are insufficient to obtain a full understanding. Electrical Capacitance Tomography (ECT) has been developed as a non-invasive measurement technique and applied to study gas-solids fluidized beds. This paper describes experiments carried out in a bench-scale fluidized bed using air and silica sand as gas-solids system. A twin-plane ECT sensor with 10 mm long measuring electrodes was designed and fabricated to study the single bubbling regime. This was based on numerical simulations to ensure that the measured capacitance values are within the detectable range of the ECT system. 2D and 3D frame-based visual analysis of bubbles formed in single bubbling regime are presented. Averaged bubble rising velocity derived by cross-correlation technique has been compared with existing empirical correlations. Good overall agreement has been found.**

***Index Terms*— Fluidized bed; electrical capacitance tomography; cross-correlation; averaged bubble velocity; electrostatic field simulation**

I. Background and Introduction

Fluidized beds are used extensively in general chemical engineering applications, such as food processing, combustion and gasification processes, drying processes or pharmaceutical industry. Their widespread use is essentially attributed to the high performance in terms of mass and heat transfer rate [1]. Despite their popularity, the inherent characteristics of fluidized beds are still not fully understood due to their complex hydrodynamic nature. Therefore novel measurement techniques are required for studying the behaviour of fluidized beds.

Generally speaking, there are two classes of measurement methods: conventional/invasive and non-invasive. Great many fundamental results have been obtained and conclusions drawn by using conventional techniques such as capacitance, fibre optic and pressure probes, which are inserted into a specific position inside of the fluidized beds. However, these tend to affect the flow processes and to some extent the results are inevitably distorted. On the other hand, non-invasive measurement techniques such as X-ray [2], Gama-ray [3] and Electrical Capacitance Tomography (ECT) [4] can obtain the desired internal properties of the gas-solids flow structures inside the fluidized bed without interfering with the flow and they have been developed significantly in recent years.

Amongst the non-invasive measurement techniques, ECT is a cost-effective way as it does not require complex support frame and space around the bed as is the case for X-ray techniques. ECT has been developed by a number of academics, a comprehensive description given in [5].The origin of the principle of ECT can be traced back to using two sets of capacitor plates to measure slug velocities. ECT system is capable of detecting the internal distribution of two phase flow, e.g. gas-solids or liquid-solids, as long as there is a dielectric permittivity difference between the two phases. In practice, the ECT sensor is mounted onto a two-phase flow rig circumferentially to measure the capacitance between each pair of measuring electrodes (normally 8 or 12 electrodes per plane) and then derive the permittivity distribution from the capacitance values by virtue of suitable reconstruction algorithms.

Because of the advantages of ECT, it has been applied by numerous researchers to investigate the flow patterns and hydrodynamic characteristics in gas-solids fluidized beds. Wang et al. [6] imaged gas bubble shape, length and coalescence in a fluidized bed in the vicinity of an air distributor plate; Makkawi and Wright [1] demonstrated an application of a twin-plane ECT system in a conventional fluidized bed and classified different flow regimes via transition velocities (the onset velocities from one flow regime to another); the influence of permittivity models on cylindrical phantom images obtained from electrical capacitance tomography has been studied by McKeen and Pugsley [7].

The sensor/electrode geometry is usually a trade-off between several factors. In principle, short electrode length helps to resolve the flow structures better in the flow direction. However, short electrodes are disadvantageous

Manuscript received 6th, March, 2016; revised 16th, April, 2016. Xiaoxu Li would like to thank China Scholarship Council (CSC) for providing his maintenance and School of Civil Engineering, Faculty of Engineering, University of Leeds for providing his tuition fees during PhD studies.

Xiaoxu Li is with Faculty of Engineering, University of Leeds, Leeds, LS2 9JT, UK; (email: cnxl@leeds.ac.uk).

Artur J. Jaworski, the corresponding author, is with the Faculty of Engineering, University of Leeds, Leeds LS2 9JT, UK; (email: a.j.jaworski@leeds.ac.uk).

Xiaoan Mao is with the Faculty of Engineering, University of Leeds, Leeds LS2 9JT, UK; (email: x.mao@leeds.ac.uk).

ISBN: 978-988-14048-0-0
ISSN: 2078-0958 (Print); ISSN: 2078-0966 (Online)

from the point of view of signal to noise ratio (and thus sensitivity). Similarly, the electrode length impacts the ability to obtain reliable cross-correlation results when studying the bubble rise velocity. In previous research the electrode length was typically 30 mm, while the imaging was limited to 100 frames per second (fps). In this paper, a twin-plane sensor with electrode length of 10 mm is designed and fabricated to investigate the bubble behaviour (especially bubble rising velocity) at 200 fps. Based on numerical simulations, this electrode length seemed a reasonable compromise between the need for short electrodes and sufficient sensitivity of ECT system available. 2D and 3D visual analysis of bubbles formed in the single bubbling regime has been presented. Cross correlation is applied to estimate averaged bubble rising velocity. Results are analysed and compared with existing empirical correlations used to estimate bubble rise velocity.

II. EXPERIMENTAL APPARATUS

Experiments have been are conducted in a fluidized bed at room temperature and atmospheric pressure. A schematic diagram of the rig used in the present study can be found in Figure 1.

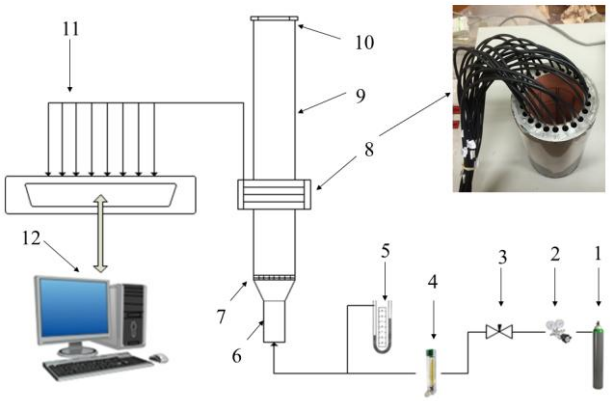

Fig. 1. Schematic diagram of experimental apparatus
1. Compressed air cylinder; 2. Air regulator; 3. Needle valve; 4. Flowmeter; 5.U-shaped manometer; 6. Plenum. 7. Air distributor; 8. Twin plane ECT sensor; 9. Fluidized bed; 10. Top cap; 11. Capacitance Measurement Unit (CMU); 12; Holding PC.

The fluidized bed consists of 1 m long acrylic pipe with 59 mm internal diameter and 3 mm wall thickness. Silica sand is used as granular material. 48 holes of 1 mm diameter are drilled in a perforated PVC distributor. The total area of the holes in the distributor is 3.768 x 10^{-5} m^2 (1.38% of the total effective area). Ambient air is provided by a compressed air cylinder. A needle valve acts as the isolation valve and controls the air flowing into fluidized bed. A float type flowmeter is used to measure superficial air velocity. To prevent silica sand from blowing out of the pipe, a customized cap in which a piece of fine mesh is embedded is mounted on top of the pipe. The static height of the fluidized bed is kept at 170 mm, which ensures that the granular material completely covers the electrodes (including guard electrodes). This is to keep the electrostatic field as two-dimensional as possible for the calibration. The density of silica sand is 2650 kg/m^3, and its mean diameter is 620 microns, which satisfies the Geldard classification of Group B particles for fluidization. Its cumulative diameter curve can be found in Figure 2, which is obtained by mechanical sieving analysis. A U-shaped water manometer is connected in the gas supply line to measure the pressure drop.

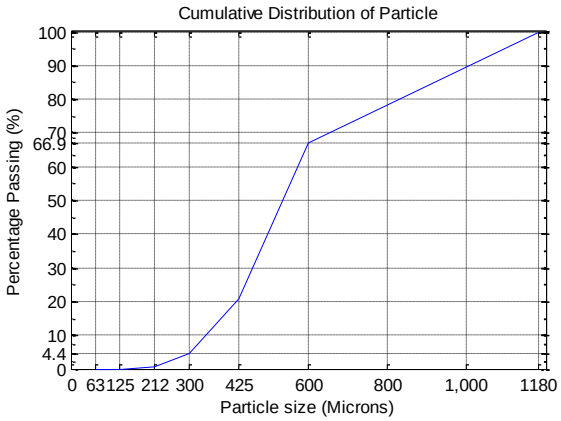

Fig. 2. Cumulative diameter curve of silica sand

The ECT system used here consists of a customized twin-plane sensor and Capacitance Measurement Unit (CMU), PTL300, from Process Tomography, Ltd, Cheshire, UK. The data capture, image reconstruction and display are done using their software, ECT32v2. The sensor has eight measuring electrodes in each plane. The electrode length is 10 mm. Three guard electrode planes are used to keep the electrostatic field two-dimensional within measurement planes. The centre-to-centre distance between measuring planes is 40 mm. The experimental details are summarised Table I.

TABLE I
EXPERIMENTAL DETAILS

Fluidized bed	59 mm ID; 3 mm wall thickness,1 m long
Particle	Silica sand, density: 2560 kg/m^3, mean diameter: 620 microns
Fluidization gas source	Ambient air, room temperature
Distributor	Perforated plate, 48 holes of 1mm diameter
ECT sensor	Sampling rate: 200 fps; 8 electrodes for each plane which is 10 mm long.
Static bed height	170 mm

III. NUMERICAL SIMULATION

During the design process, it is important to simulate the inter-electrode capacitance values between each pair of measuring electrodes to ensure the measured capacitance values are in the detectable range of the ECT system. COMSOL Multiphysics (version 4.4; Electrostatics Field AC/DC module) has been used for simulating the electrostatic field within the sensor and calculating the resulting capacitance values [8]. The relationship between capacitance and permittivity distribution is governed by the following equation [9]:

$$C = \frac{Q}{V_C} = \frac{\oint_S \varepsilon(x,y)\nabla\varphi(x,y)ds}{V_C} \quad (1)$$

where ε(x, y) is the permittivity distribution in the sensing field, V_c is the potential difference between two electrodes

ISBN: 978-988-14048-0-0
ISSN: 2078-0958 (Print); ISSN: 2078-0966 (Online)

forming the capacitance, φ(x, y) is the potential distribution and S is the closed line surrounding the electrode.

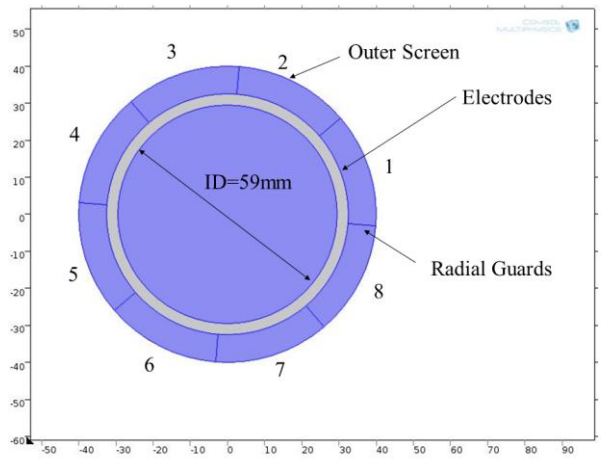

Fig. 3. Schematic diagram of COMSOL simulation geometry

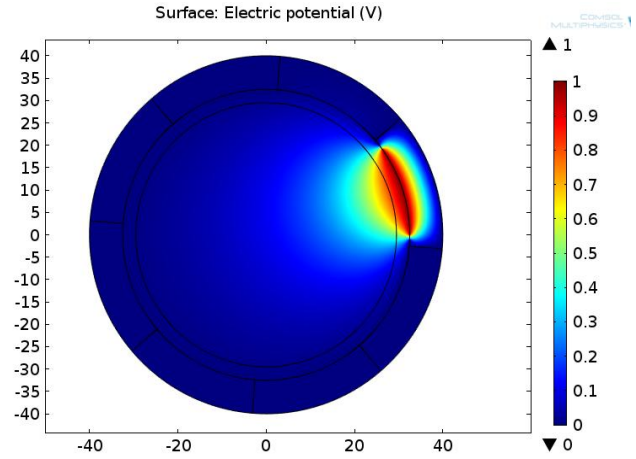

Fig. 4. Typical electrical potential distribution when one electrode is 'excited'.

A schematic diagram of the sensor geometry can be found in Figure 3. Eight electrodes are distributed circumferentially around a pipe that has an outer diameter of 65 mm and 3 mm wall thickness. Numbering of electrodes starts at ''3 o'clock'' in anti-clockwise direction. Figure 4 shows an example of potential distribution when electrode 1 is ''excited'' and the remaining electrodes work as ''detectors''. Two extreme conditions are simulated. Firstly, the area within the pipe is fully occupied by air (permittivity of 1 is applied); and then, only silica sand (permittivity of 3.0 is applied) fills the pipe area. Capacitance values of these two conditions for each pair of electrodes are obtained. Since the electrostatic field is symmetrical, only electrode pairs of 1-2, 1-3, 1-4 and 1-5 are shown here in Table II. The capacitance values between adjacent electrodes are much higher than pairs of the opposite electrodes, which can be explained by equation (1). Also the values, when the pipe is full of silica sand, are significantly higher than the empty pipe. The higher permittivity of silica sand contributes to this difference. As the measurement range of the ECT system is 0.1fF – 2000fF, the simulated capacitance values from Table II are all within the above range.

TABLE II.
SIMULATED CAPACITANCE VALUES BASED ON 10 MM LONG MEASURING ELECTRODES

Pairs	Capacitance with air (fF)	Capacitance with silica sand (fF)
1-2	101.39	168.46
1-3	7.87	23.28
1-4	4.31	12.87
1-5	3.63	10.86

IV. RESULTS AND DISCUSSIONS

A. Pressure drop and Minimum Fluidization Velocity (MFV) determination

Pressure drop across the fluidized bed is an essential parameter in determining the onset of fluidization. The corresponding superficial velocity is referred as Minimum Fluidization Velocity (MFV). A simple U-shaped manometer connected to the plenum can detect the point of incipient fluidization as the point of a local decrease of the pressure drop when plotted as a function of superficial velocity. Clearly, the pressure drop reading at fluidization regime exhibits fluctuation and this can be reasonably eliminated by averaging the reading. According to Figure 5, the minimum fluidization velocity is 0.174 m/s while the corresponding pressure drop at that point is 3996.2 Pa.

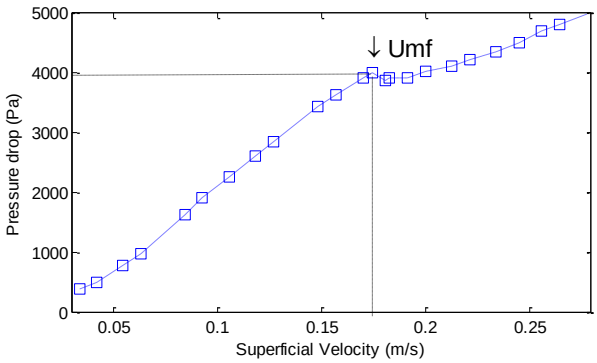

Fig. 5. Relationship between pressure drop across fluidized bed and superficial velocity.

B. Frame-based Analysis

Although a transparent acrylic pipe is used in constructing a fluidized bed, direct visual observation is still hindered by the three dimensional nature of the bed. It is advantageous to use ECT techniques with fast cross-sectional imaging which can produce series of frames at a sampling rate up to 200Hz. A typical frame by frame images at both measuring planes are displayed in the upper two rows (first row for plane 1, second row for plane 2) in Figure 6 when the superficial velocity is at a medium level (Uo=0.22m/s). The interval between consecutive images is 0.05s (corresponding to 200 Hz sampling rate). Therefore the duration from the first to the sixth image for each plane is 0.3 s. It can be seen from the six images from plane 1 that a bubble starts to appear in image 2, grows until image 4 and decays for image 5. A similar trend can be found in plane 2 and a slight bubble size growth can be observed when comparing the overall bubble size at plane 1. This is in line with previous bubble growth findings in literature. It is worth noting that the images in

ISBN: 978-988-14048-0-0
ISSN: 2078-0958 (Print); ISSN: 2078-0966 (Online)

plane 2 are deliberately shifted to be aligned with Plane 1. In reality there is a larger time delay, and this can be derived by cross-correlation techniques, which will be explained in detail in Section C. In order to identify how the bubbles develop in a single bubbling regime, three frames for three different superficial velocities are displayed at the third row of Figure 6. These three frames are selected based on the local maximum volume ratio, which are calculated by normalised capacitance values. The blue area in the frames can be regarded as the maximum bubble size when the bubbles are passing plane 2. It can be concluded that the maximum bubble size is growing with the increasing superficial velocity from 0.18 m/s to 0.26 m/s. The location of the bubbles within the cross-sectional area is actually random, i.e. sometimes they are attached around wall and sometimes they appear in the centre – the shape of the bubbles can be semi-spherical, which is attributed to the wall effect.

A pseudo 3D 'train' of a series of cross sectional frames generated can be seen in Figure 7. This figure is plotted based on the superficial velocity of 0.26 m/s. In this 3D image, it can be seen that the bubble is rising along an axis between wall and centreline of the bed and is approximately spherical. Although not much quantitative information can be extracted from the frame-based analysis, it can still support the experimental measurements and aid the further quantitative analysis.

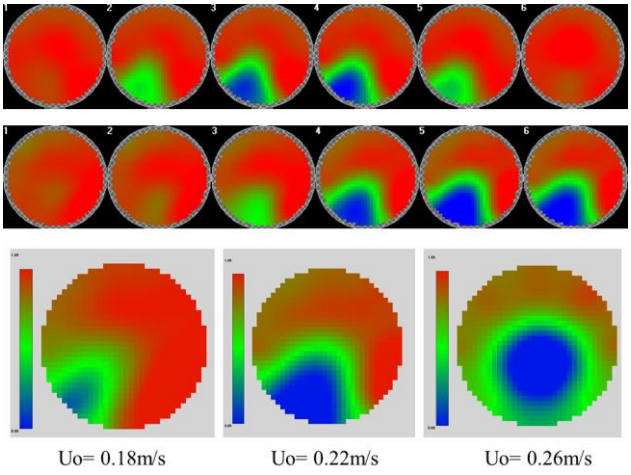

Fig. 6. A typical frame-based analysis obtained by ECT software.

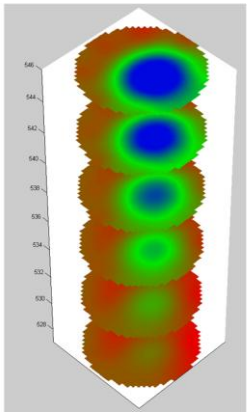

Fig. 7. A typical pseudo 3D 'train' of a series of cross sectional frames obtained by ECT software.

C. *Averaged bubble rising velocity estimation*

Cross-correlation techniques are useful in investigating pipeline flow velocity. Here, they can be used to derive the time delay of a bubble travelling from the lower to the upper ECT plane. The average bubble rising velocity could be obtained providing the distance between these two planes is known.

$$R_{xy}(\tau)=\frac{1}{T}\int_0^T X(t)Y(t+\tau)dt \tag{2}$$

where X(t), Y(t) are the signal from lower and upper measuring planes; τ time delay; T the integration time.
The above equation can be written in discrete form as follows:

$$R_{xy},k(j)=\frac{1}{N}\sum_{i=1}^{N}x_k(i)\,y_k(i+j) \tag{3}$$

where j=0,1,2,…,M; k=1,2,…,812; x(i) and y(i) are the upper and lower plane signals, N is the number of samples in the summation, M is the number of samples in cross correlation calculation, j is the number of delayed samples, and k is the pixel index.

In the present work, a twin plane ECT sensor is designed to be able to estimate the averaged bubble rising velocity with a centre to centre distance of 40 mm. Once the time delay is established (by finding the time for which the correlation function is maximum) an averaged bubbling rising velocity is achieved when the distance between two measuring planes is divided by the time delay

From the acquired ECT images it is clear that the cross-sectional position of the bubbles varies – some passing near the pipe centre, others nearer the wall (e.g. see Figure 6). The entire image area is composed of 812 pixels. However, to investigate the bubble behaviour five pixels are selected for convenience. They are pixels (1, 16), (16, 1), (16, 16), (16, 32), (32, 16), as marked in Figure. 8. Three different methods are applied to implement this process.

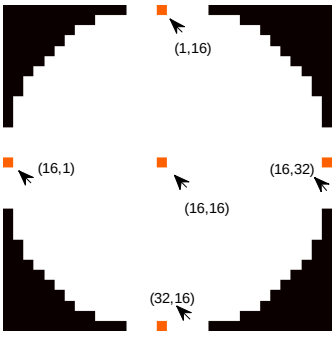

Fig. 8. Five selected point's relative position in the cross section of the ECT image.

Firstly, as solid fraction based on pixel's grey level is the most straightforward data which can be acquired from ECT measurements. The solid fraction for the five selected points is plotted in Figure 9 as a function of time. The figure shows typical plane 2 solid fraction plots for time interval of 2.5 seconds (starting from 2.5 s to 5 s) with three different superficial velocities (Uo=0.18m/s, 0.22m/s and 0.26m/s) for the five representative points.

ISBN: 978-988-14048-0-0
ISSN: 2078-0958 (Print); ISSN: 2078-0966 (Online)

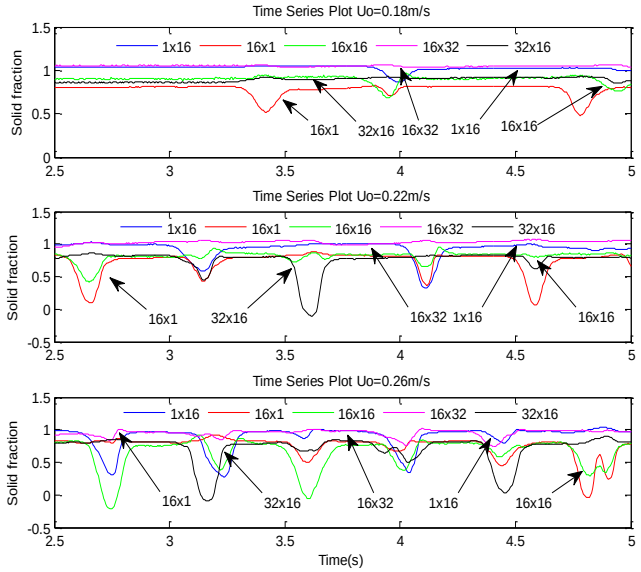

Fig. 9. Solid fraction of the five selected points within a period of 2.5 second with different superficial velocity.

It is commonly accepted that a sudden decrease on solid fraction can be regarded as the appearance of a bubble. When superficial velocity is at 0.18m/s, bubbles appear strongly around point (1,16), point (16,1) and point (16,16). Points (16,32) and (32,16), however, have a nearly flat solid fraction, i.e. there are no sizable bubbles passing these pixels. With the increased superficial velocity from 0.18 m/s to 0.26 m/s, the profile of all of the five points indicates bubbles equally randomly appearing across the cross section, although point (16x32) still does not exhibit bubble presence when superficial velocity is 0.22 m/s .

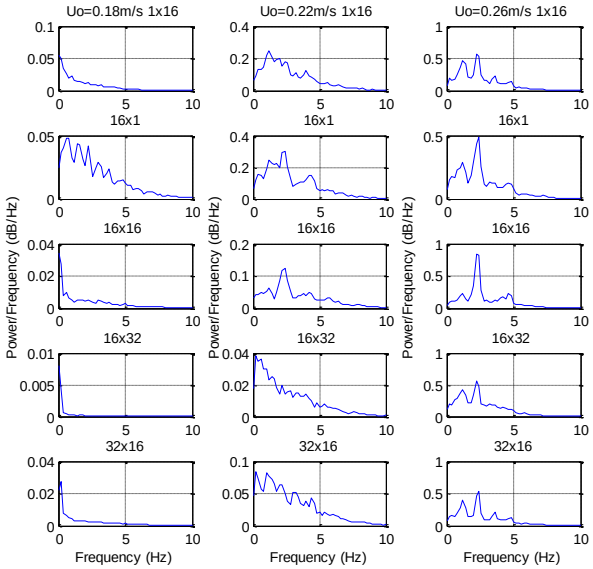

Fig. 10. Power Spectral Density (with a sampling volume of 16000 frames) of the five selected points at three different superficial velocity (Uo=0.18m/s, 0.22m/s and 0.26m/s).

Secondly, Power Spectral Density (PSD) is an effective frequency domain approach in fluidized bed investigation. In this part, PSD is used to assist in examining the five points' response. Again, plane 2 data is applied to produce PSD results to ensure the dataset is consistent with solid fraction analysis. PSD results at three different superficial velocities are displayed in three columns in Figure 10 – each column contains the results for five points. Dominant frequency in PSD is commonly regarded as the averaged bubbling frequency. At the first column, except the point (16,1), the dominant frequency for other four points take place near the frequency of zero, which indicates rare and weak bubble presence around these points. This phenomenon is in line with the solid fraction analysis where point (16,1) gives a strongest solid fraction when bubble appears when the superficial velocity is at 0.18m/s. With the superficial velocity increased to Uo=0.26 m/s, dominant frequency of the five points all occur around 2.3 Hz. This result has an acceptable agreement with the solid fraction analysis under the same superficial velocity where 6 bubbles emerge in 2.5 second (giving a bubble frequency at 2.4 Hz).

Finally, to finalise examining these five points, cross correlation is executed. The results of time lag for averaged bubble rising velocity at three different velocities are summarised in Table III. Negative value means that the signal at plane 2 is delayed compared with plane 1. Zero value means there is no correlated time lag available as the signals from these two planes cannot be correlated in practice. As it can be seen, point (16,32) can hardly have correlated time lag until the superficial velocity is increased to 0.26 m/s, which is consistent with solid fraction and PSD analysis.

TABLE III.
CROSS-CORRELATION TIME LAG AT THREE DIFFERENT SUPERFICIAL VELOCITIES FOR THE FIVE SELECTED POINTS (UNIT: S)

Position	Superficial Velocity		
	0.18m/s	0.22m/s	0.26m/s
Point (1,16)	0	-0.11	-0.115
Point (16,1)	-0.155	-0.115	-0.11
Point (16,16)	0	-0.11	-0.105
Point (16,32)	0	0	-0.115
Point (32,16)	0	-0.115	-0.105

To have a more extensive understanding of the bubble rising velocity, cross-correlation results of these five points can be compared with empirical correlations. Numerous empirical bubble rising velocity estimation correlations are available in the literature. In this work, two widely referenced correlations from Werther and Davidson [10,11] are selected as these are also regarded as the best ones for estimating bubble rising velocity by Karimipour and Pugsley [12], based on their squared difference analysis between the experimental data and correlation results. In Werther's correlation, a bubble size correlation is also required, which can be found as follows. The bubble size correlation is also derived by Werther.

$$U_b = \varphi\sqrt{g\,d_b} \tag{4}$$

$$d_b = d_0[1+0.272(U_0-U_{mf})]^{1/3}(1+0.0684h)^{1.21} \tag{5}$$

For Geldart B particles: φ=0.64 if D<=10; φ=0.254D$^{0.4}$ if 10=<D<=100; φ=1.6 if D>=100; d_0=0.853 for Gerldart B particles; D is the diameter of fluidized bed.

$$U_b = U_{br} + (U_0 - U_{mf}) \tag{6}$$

$$U_{br} = 0.71\sqrt{g\,d_b} \tag{7}$$

However, in Davidson's correlation, there is no bubble size estimation correlation provided with the corresponding

ISBN: 978-988-14048-0-0
ISSN: 2078-0958 (Print); ISSN: 2078-0966 (Online)

bubble rising velocity correlation. Hence, an empirical bubble size correlation from Mori [13] which is generally accepted is used. Averaged bubble rising velocity comparison between results extracted by cross-correlation for the five points and Werther's and Davidson's correlations is shown in Figure 11.

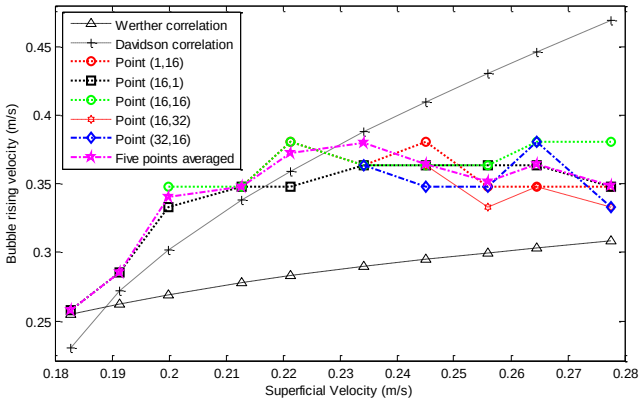

Fig. 11. Bubble rising velocity results. Comparison between ECT cross correlation results and Werther's and Davidson's correlations.

Overall, the results between cross-correlation and empirical correlation have a good agreement. When the superficial velocity increases, the averaged bubble rising velocity also increases. Results from the cross-correlation for the five points lie in between the two empirical correlations when the superficial velocity is more than 0.22m/s. This confirms that the cross-correlation technique is a reliable approach in estimating bubble rising velocity with ECT measurements. However, it can be found by comparing the results between Werther's and Davidson's correlations that Davidson's results are much higher than Werther's especially when the superficial velocity is more than 0.2m/s. This fact can be attributed to the term of U_o-U_{mf} in Davidson's correlation which does not appear in Werther's correlation. As U_{mf} is constant, when the superficial velocity increases, the difference of U_o-U_{mf} is correspondingly increased. It is worth noting that the five points start to have more equally random bubble appearance when the superficial velocity is more than 0.23 m/s. The heterogeneity of granular material could attribute to this when the superficial velocity is lower. According to the cumulative diameter curve, the distribution of the particle's diameter is quite diverse from its mean value of 620 um. The introduced gas could preferentially take the path through smaller diameter particles which may exert lower resistance force. This can be confirmed in future by applying a more concentrated granular material.

By observing the results from cross-correlation for the five selected points it can be seen that the bubble rising velocity is steadily increasing when the superficial velocity is increasing from 0.18m/s to 0.24m/s. However, by viewing the five points' results and their averaged bubble rising velocity one, this trend is slightly heading down when the superficial velocity is more than 0.26 m/s whilst two empirical results increase continually. This is probably caused by the slugging regime effect. Through visual observation of the fluidization process, it can be seen that when the superficial velocity is more than 0.26m/s, the bed expands significantly and the bubble size is large enough to cover more than half of the cross section of the bed, which can be treated as slug. With the increasing bubble volume, the corresponding bubble or slug rising velocity is decreased.

V. CONCLUSIONS

Electrical Capacitance Tomography (ECT) has been developed as a non-invasive measurement technique and applied to study gas-solids fluidized beds. This paper describes experiments carried out in a bench-scale fluidized bed using air and silica sand as gas-solids system. A twin-plane ECT sensor with 10 mm long measuring electrodes was designed and fabricated to study the single bubbling regime. This was based on numerical simulations to ensure that the measured capacitance values are within the detectable range of the ECT system. 2D and 3D frame-based analysis of bubbles formed in single bubbling regime are presented. Averaged bubble rising velocities were obtained from cross-correlation technique for five selected points and these were compared with existing empirical correlations. Good trend agreement has been found. Future work will focus on the effect of different reconstruction algorithms, permittivity model and data acquisition rate on bubble size estimation in order to gain a more comprehensive understanding of bubble behaviour.

REFERENCES

[1] Makkawi, Y.T. and P.C. Wright, Electrical capacitance tomography for conventional fluidized bed measurements—remarks on the measuring technique. *Powder technology*, 2004. 148(2): p. 142-157.
[2] Rowe, P. and B. Partridge, An x-ray study of bubbles in fluidised beds. *Transactions of the Institution of Chemical Engineers*, 1965. 43: p. 157-165.
[3] Weimer, A., D. Gyure, and D. Clough, Application of a gamma-radiation density gauge for determining hydrodynamic properties of fluidized beds. *Powder technology*, 1985. 44(2): p. 179-194.
[4] Halow, J., et al., Observations of a fluidized bed using capacitance imaging. *Chemical Engineering Science*, 1993. 48(4): p. 643-659.
[5] Williams, Richard Andrew, and Maurice S. Beck, eds. Process tomography: principles, techniques, and applications. Butterworth-Heinemann, 1995.
[6] Wang, S., et al., Real time capacitance imaging of bubble formation at the distributor of a fluidized bed. *The Chemical Engineering Journal and the Biochemical Engineering Journal*, 1995. 56(3): p. 95-100.
[7] McKeen, T.R. and T.S. Pugsley, The influence of permittivity models on phantom images obtained from electrical capacitance tomography. *Measurement Science and technology*, 2002. 13(12): p. 1822.
[8] Jaworski, A. J., and G. T. Bolton. "The design of an electrical capacitance tomography sensor for use with media of high dielectric permittivity." *Measurement Science and Technology* 2000. 11(6): 743.
[9] Jaworski A. J, Meng G. On-line measurement of separation dynamics in primary gas/oil/water separators: challenges and technical solutions—a review. *Journal of Petroleum Science and Engineering*. 2009 Sep 30;68(1):47-59.
[10] Werther J. Effect of gas distributor on the hydrodynamics of gas fluidized beds. *German Chemical Engineering*. 1978;1:166-74.
[11] Davidson, John Frank, Roland Clift, and David Harrison. "Fluidization." (1985).
[12] Karimipour, S. and T. Pugsley, A critical evaluation of literature correlations for predicting bubble size and velocity in gas–solid fluidized beds. *Powder Technology*, 2011. 205(1): p. 1-14.
[13] Mori S, Wen CY. Estimation of bubble diameter in gaseous fluidized beds. *AIChE Journal*. 1975 Jan 1;21(1):109-15.

ISBN: 978-988-14048-0-0
ISSN: 2078-0958 (Print); ISSN: 2078-0966 (Online)